

# Tricolor Visible Wavelength-selective Photodegradable Hydrogel Biomaterials

Teresa L. Rapp<sup>1</sup> & Cole A. DeForest<sup>\*1-5</sup>

## Affiliations:

<sup>1</sup>Department of Chemical Engineering, University of Washington, Seattle, WA 98195, USA.

<sup>2</sup>Department of Bioengineering, University of Washington, Seattle, WA 98195, USA.

<sup>3</sup>Department of Chemistry, University of Washington, Seattle, WA 98195, USA.

<sup>4</sup>Institute of Stem Cell & Regenerative Medicine, University of Washington, Seattle, WA 98109, USA.

<sup>5</sup>Molecular Engineering & Sciences Institute, University of Washington, Seattle, WA 98195, USA.

\*Correspondence to: [profcole@uw.edu](mailto:profcole@uw.edu)

## ORCID:

**Rapp:** <https://orcid.org/0000-0002-4775-7604>

**DeForest:** <https://orcid.org/0000-0003-0337-3577>

## **Abstract:**

Photodynamic hydrogel biomaterials have demonstrated great potential for user-triggered therapeutic release, patterned organoid development, and 4D control over advanced cell fates in vitro. Current photosensitive materials are constrained by their reliance on high-energy ultraviolet (UV) light (<400 nm) that offers poor tissue penetrance and limits access to the broader visible spectrum. Here, we report a family of three photolabile material crosslinkers that respond rapidly and with unique tricolor wavelength-selectivity to low-energy visible light (400 – 617 nm). When mixed with multifunctional poly(ethylene glycol) macromolecular precursors, novel ruthenium polypyridyl- and *ortho*-nitrobenzyl (*o*NB)-based crosslinkers yield cytocompatible biomaterials that can undergo spatiotemporally patterned, uniform bulk softening, and multiplexed degradation several centimeters deep through complex tissue. Encapsulated living cells within these photoresponsive gels show high viability (>85%) and can be successfully recovered from the hydrogels following photodegradation. Moving forward, we anticipate that these advanced material platforms will enable new studies in 3D mechanobiology, controlled drug delivery, and next-generation tissue engineering applications.

## **Introduction:**

Light is a particularly powerful stimulus for gaining spatiotemporal control over dynamic material transformations. In contrast to intrinsic stimuli such as pH, temperature, and protease levels that are challenging to regulate in a biological setting, light's ability to be precisely administered affords unique control over when, where, and to what degree materials undergo pre-programmed responses as well as a route to sidestep challenges associated with patient-to-patient variability in clinical applications. Recognizing this unique utility, the biomaterials community has invested substantial efforts towards the development of photoresponsive hydrogels – water-swollen polymer networks that elicit a prespecified change upon directed light irradiation<sup>1-4</sup>. The resulting systems have driven significant advances across multiple fields, including cellular biology<sup>5-10</sup>, drug discovery<sup>11-15</sup>, tissue engineering platforms for directing cell fate<sup>16,17</sup>, and the formation of organoids<sup>18,19</sup>. Photodynamic hydrogels take advantage of light's spatiotemporal control to trigger photoinduced material softening<sup>20,21</sup>, biochemical release<sup>22-24</sup>, and species uncaging/activation for *in vivo* material modification<sup>25</sup>.

Despite the early promise of phototunable gels, chemistry- and material-based limitations have precluded the full power of these platforms from being realized<sup>2</sup>. Reliance on organic chromophores to encode photodegradability within hydrogels has historically confined the photocleaving wavelengths to high-energy light – ranging from  $\leq 365$  nm for *ortho*-nitrobenzyl (oNB)-based systems up to 450 nm for some reported photolabile coumarins and bimanes<sup>26-28</sup>. While some of these chromophores have been highly characterized and are cytocompatible throughout photolysis, the utilization of UV light irradiation has traditionally confined these materials to solely *in vitro* use as high-energy light is poorly penetrant through complex

tissue<sup>3,29</sup>. Additionally, only a limited number of reports have described materials that are sensitive to multiple orthogonal wavelengths, of which nearly all crosslinkers employed rely heavily on near- and far-UV light<sup>27,28,30-33</sup>, thereby missing significant opportunities for cytocompatible material multiplexing by taking advantage of the entire spectrum of visible and IR light. A collection of photocleavable crosslinkers that distinctly responds to an expanded portion of electromagnetic spectrum, enabling deeper tissue penetration and multiplexed wavelength-selective material modulation using differently colored light, would enable exciting new directions for phototunable hydrogel platforms.

Seeking to expand light response into the visible range, we turned our attention towards ruthenium (Ru) polypyridyl complexes, which continue to gain new and unique ground in the world of photochemistry<sup>34,35</sup>. These compounds are highly photoactive and undergo covalent bond breakage upon visible light irradiation, with quantum yields of photodissociation many times greater than current organic chromophores and reaching 0.1 – 0.6 in many cases<sup>36-38</sup>. Capitalizing on these advances, Ru complexes have found utility in the biochemical space as photocaging groups<sup>35,39,40</sup> and in the generation of photoresponsive micelles for drug delivery<sup>41</sup>. Though most ruthenium compounds bearing 2,2'-bipyridine ligands commonly absorb blue light (420 – 450 nm), comparatively simple syntheses can yield species with shifted absorbances extending into the red and near-IR<sup>42,43</sup>. With their radical-free ligand exchange<sup>40</sup>, engineered cytocompatibility, and high photoefficiency, we postulated that uniquely visible light-responsive biomaterials could be created through direct inclusion of such Ru complexes in a polymer backbone, providing a route to next-generation photodynamic hydrogels.

In this work, we describe the synthesis and properties of a new series of photolabile crosslinkers, including two based on novel ruthenium compounds: (1) Ru(2,2'-biquinoline)<sub>2</sub>(4-azidobutanenitrile)<sub>2</sub> (denoted **Rubiq**); (2) (Ru(2,2'-bipyridine)<sub>2</sub>(4-azidobutanenitrile)<sub>2</sub> (**Rubpy**); and (3) an established **oNB**<sup>44</sup> with wavelength-separated  $\lambda_{\max}$  capable of respectively responding selectively to three different colors of visible light – red (617 nm), green (530 nm), and blue (405 nm) (**Fig. 1a,b**). Mixing four-arm poly(ethylene glycol) (PEG) end-functionalized with bicyclononyne (PEG-tetraBCN) together with the bis(azide)-modified photolinkers with 1:1 stoichiometry with respect to their reactive groups, idealized step-growth polymeric gels can be readily formed through bioorthogonal strain-promoted azide-alkyne cycloaddition (SPAAC) (**Fig. 1c**)<sup>45</sup>. Taking advantage of crosslinkers designed to rapidly photolyze in a cytocompatible and visible wavelength-selective manner, we anticipated being able to achieve multiplexed material degradation in the presence of living cells and through complex tissue.

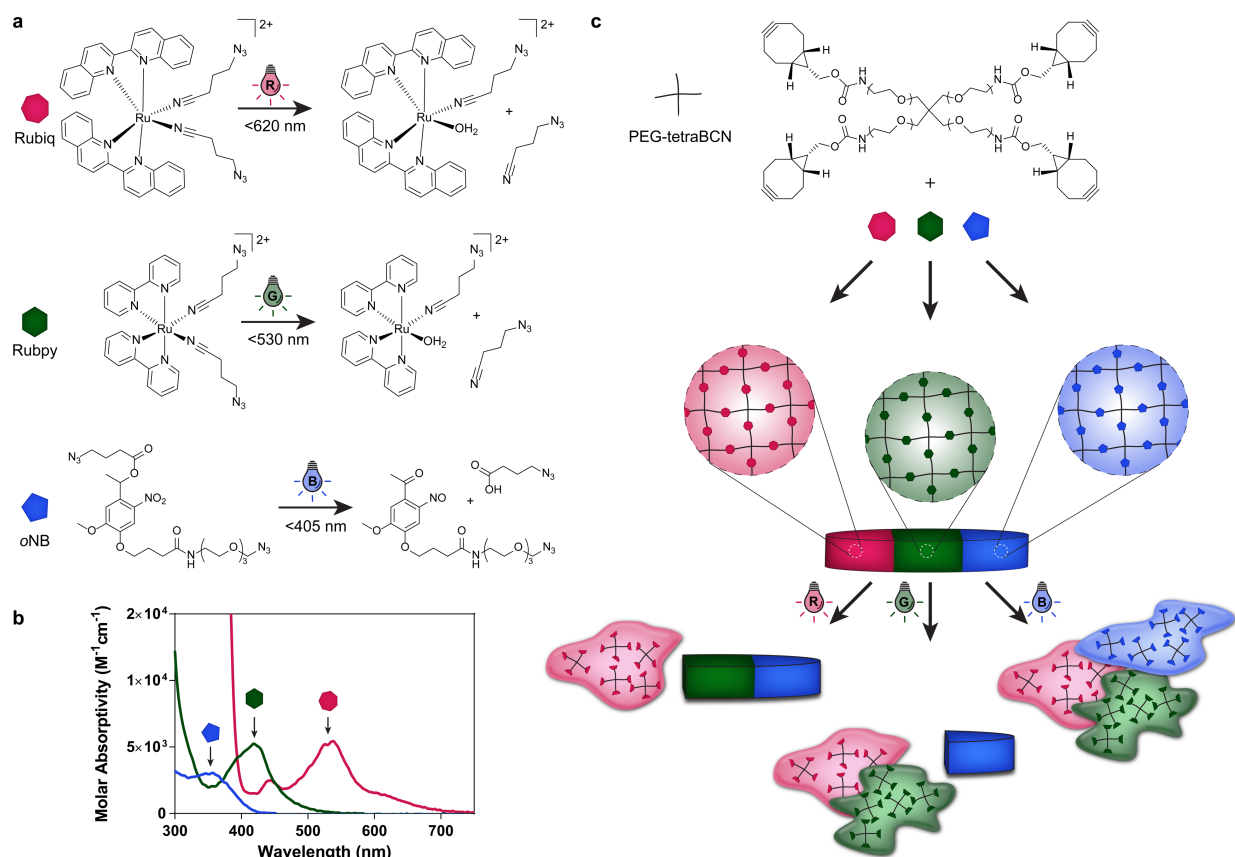


**Figure 1 | Photodegradable crosslinkers cleave in a visible wavelength-selective manner. a.** Novel crosslinkers **Rubiq** (pink heptagon), **Rubpy** (green hexagon), and **oNB** (blue pentagon) undergo photolysis. Upon absorption of a photon, each ruthenium complex undergoes ligand exchange via population of a triplet metal-centered state via intersystem crossing from the low lying metal-to-ligand charge transfer (MLCT) band. This results in radical-free metal-ligand bond cleavage. Crosslinkers are modified with two azides for direct incorporation into hydrogel networks. **b.** Absorbance spectra of **Rubiq**, **Rubpy**, and **oNB**. Each crosslinker exhibits an extended absorbance spectrum beyond their  $\lambda_{\text{max}}$  permitting excitation at wavelengths lower than  $\lambda_{\text{max}}$ . **c.** PEG-based hydrogel formation occurs spontaneously upon mixing each crosslinker with 4-arm PEG-BCN via strain-promoted azide-alkyne cycloaddition. Resulting hydrogels degrade under red, green, or blue light with perfect unidirectional orthogonality ( $>617 \text{ nm}$  for **Rubiq**,  $>530 \text{ nm}$  for **Rubpy**, and  $>405 \text{ nm}$  for **oNB**).

## **Results:**

### **Synthesis and photochemical characterization of Rubiq, Rubpy, and *o*NB-based crosslinkers**

Photolabile crosslinkers were each synthesized with flanking azides, permitting their incorporation into bulk hydrogels via SPAAC. **Rubiq** and **Rubpy** were respectively synthesized in a two- and one-step processes from Ru(bpy)<sub>2</sub>Cl<sub>2</sub> or RuCl<sub>3</sub> and 2,2'-biquinoline, whereby azide-bearing ligands (4-azidobutanenitrile) were coordinated to form symmetrical Ru-based crosslinkers. The bis(azide) ***o*NB** was synthesized following published protocol with minimal changes<sup>44</sup> (see Methods for synthetic details). All crosslinkers were synthesized, purified, and chemically characterized with appreciable yields (**Rubiq**: 27%, **Rubpy**: 77%, ***o*NB**: 17% overall yield).

Upon irradiation with the appropriate wavelengths of light, **Rubiq** and **Rubpy** undergo ligand exchange with a solvent molecule (in this case, water) due to population of a metal-centered antibonding orbital (**Fig. 1a, Supplementary Fig. 1**). **Rubiq** and **Rubpy** exhibit low-energy absorbance bands due to low-lying metal-to-ligand charge transfer (MLCT) states common in ruthenium polypyridyl complexes<sup>46</sup>. As expected, the extended pi bond structure of 2,2'-biquinoline gave a bathochromic shift in peak absorbance of Rubiq to a  $\lambda_{\text{max}}$  of 535 nm, significantly red-shifted when compared with the 2,2'-bipyridine-containing **Rubpy** compound and ***o*NB**<sup>47</sup>. All crosslinkers exhibited a significant  $\lambda_{\text{max}}$  with a slow decay in absorptivity, permitting off-peak photon absorbance and population of antibonding orbitals at low energies (**Fig. 2a.**). For this study, **Rubiq** was photocleaved using 617 nm ( $\epsilon = 43 \text{ M}^{-1}\text{cm}^{-1}$ ), **Rubpy** with 530 nm ( $\epsilon = 14 \text{ M}^{-1}\text{cm}^{-1}$ ), and ***o*NB** at 405 nm ( $\epsilon = 118 \text{ M}^{-1}\text{cm}^{-1}$ ), wavelengths commonly

accessible through inexpensive LED light sources that balanced photocleavage efficiency and spectral separation.

This series of crosslinkers was shown to be unidirectionally orthogonal: red light (617 nm) irradiation led to photolysis of **Rubiq** only, green light (530 nm) irradiation photolyzed both **Rubiq** and **Rubpy** but left **oNB** intact, and blue light (405 nm) photolyzed all three crosslinkers (**Fig. 2a**). This is demonstrated by the presence or absence of a shift in absorbance spectrum upon irradiation; all three compounds undergo a change in their electronic structure upon photolysis which is reflected in the absorbance spectra. The insensitivity of **Rubpy** to high doses of red light, as well as **oNB** to extended exposure to red and green light, demonstrates wavelength selectivity of the small molecule crosslinkers in situ.

The appearance of a new absorbance maximum of photoproducts was used to determine the quantum yield (QY) of photocleavage at the wavelengths used in this study (**Fig. 2b, Table 1**). Light at 617 nm, 530 nm, and 405 nm at 5, 10, and 20 mW cm<sup>-2</sup> were used for the QY determination. As expected, faster photocleavage for each compound accompanied higher light intensities. When extent of photolysis was normalized to total light dosage (i.e., the product of intensity and exposure time), cleavage traces collapsed onto a single curve for each species (**Fig. 2b**). **Rubpy** has the highest QY of the three ( $0.29 \pm 0.04$ ), consistent with prior reports for Ru(bpy)<sub>2</sub>L<sub>2</sub> complexes under visible light irradiation<sup>30,37,48</sup>. **Rubiq**'s QY ( $0.016 \pm 0.009$ ) was found to be lower than that of **Rubpy**, due to the bathochromic shift decreasing intersystem crossover efficiency into the metal-centered antibonding orbital<sup>47</sup>. Though **oNB** has a very low QY at 405 nm ( $0.004 \pm 0.003$ ), its higher molar absorptivity enables photocleavage under visible

irradiation with reasonable efficiency. Finding photolysis to be complete for all three crosslinkers within 30 minutes at  $10 \text{ mW cm}^{-2}$  intensity (**Fig. 2b**), these irradiation conditions were used for all gel degradation experiments. Significant color change accompanied photolysis for each compound, particularly for **Rubiq**, providing a useful handle for qualitative crosslinker cleavage determination in hydrogel formulations (**Fig. 2c**).

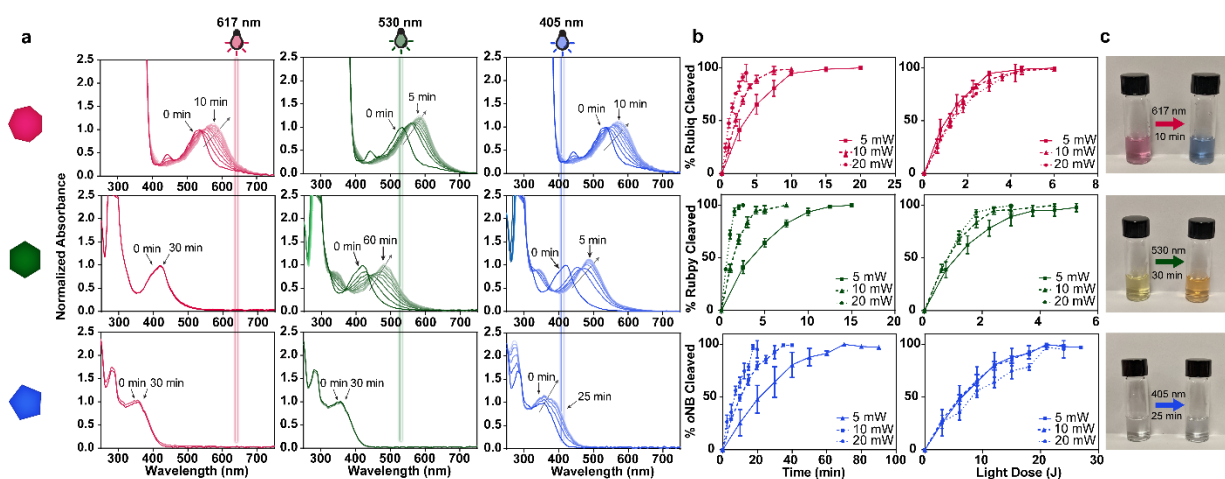


**Figure 2 | Photolabile crosslinkers can be selectively cleaved with differently colored visible light.** **a.** **Rubiq** (pink heptagon), **Rubpy** (green hexagon), and **oNB** (blue pentagon) individually subjected to 617, 530, and 405 nm light ( $10 \text{ mW cm}^{-2}$ , 0 – 60 min) undergo wavelength-selective photolysis, indicated by absorbance spectral changes. **b.** Photolysis proceeds efficiently with varied power (5, 10, 20 mW) in a light dose-dependent manner. Here, light dosage is calculated as the product of light intensity and exposure time. **c.** Color change was observed for **Rubiq** and **Rubpy** upon irradiation (10 mW, varied wavelengths and exposure times) due to the significant absorbance shift following ligand exchange.

Compound	$\lambda_{\text{max}}$ (nm)	$\lambda_{\text{excitation}}$ (nm)	Quantum Yield ( $\Phi_{\text{pr}}$ )	Molar Absorptivity ( $\epsilon, \text{M}^{-1}\text{cm}^{-1}$ )	Efficiency ( $\Phi \cdot \epsilon$ )
<b>Rubiq</b>	535	617	$0.016 \pm 0.009$	43	0.688
<b>Rubpy</b>	420	530	$0.29 \pm 0.04$	14	4.06
<b>oNB</b>	365	405	$0.004 \pm 0.003$	118	0.472

## Multiplexed hydrogel degradation via visible light irradiation

Having demonstrated the wavelength orthogonality and high efficiency of this series of photocleavable molecules, we sought to employ them as crosslinkers in PEG-based hydrogel systems. To create visible light-degradable hydrogels, **Rubiq**, **Rubpy**, and **oNB** were polymerized with PEG-tetraBCN via SPAAC chemistry (**Fig 3a**). Though gelation kinetics varied slightly with crosslinker identity, each formulation resulted in equivalently stiff hydrogels ( $G' \sim 2.5$  kPa), as quantified using in situ rheometry (**Fig 3b**). Following complete gelation, hydrogels crosslinked with **Rubiq**, **Rubpy**, and **oNB** were individually subjected to sequential treatments (35 min each) of 617 nm, 530 nm, and 405 nm light ( $10 \text{ mW cm}^{-2}$ ), with photodegradation assessed rheometrically. **Rubiq**-based gels degraded rapidly upon red light illumination, while those containing **Rubpy** and **oNB** persisted; **Rubpy** subsequently degraded with green light with **oNB** materials unchanged; finally, blue light afforded rapid cleavage of the remaining **oNB**-crosslinked hydrogel (**Fig. 3c**). Results highlight that the gels can be photodegraded in a visible wavelength-selective manner as designed.

To access intermediate bulk hydrogel stiffnesses, hydrogels were cast with equal amounts of the photolabile crosslinkers (i.e., 1:1:1 **Rubiq:Rubpy:oNB**) alongside varied percentages (0 – 90%) of photostable diazido-tri(ethylene glycol) crosslinker (denoted TEG), while keeping the total crosslinker concentration constant (**Fig. 3d, Supplementary Fig. 2**). When sequentially subjected to red, green, and blue light ( $10 \text{ mW cm}^{-2}$ , 35 min each) and analyzed rheometrically, hydrogels partially softened to intermediate moduli or fully degraded in a manner dependent on crosslinker makeup and wavelength-selectivity. Consistent with polymer network rubber elasticity theory, the incorporation of stable TEG crosslinks into the matrix at varying

percentages stabilized the hydrogel at intermediate stiffness following complete lysis of photocleavable crosslinks. Hydrogels with low percentages of TEG (10%) lost all elastic properties after exposure to red + green light, matching Flory-Stockmeyer predictions that ~60% of the available crosslinks must remain intact for the gel to persist (remaining *o*NB + TEG crosslinks  $\approx$  40% of available crosslinks). When TEG comprised >60% of crosslinks, the hydrogel was no longer fully photodegradable, yielding a soft stable hydrogel following complete light treatment, further predicted through Flory-Stockmayer analysis (**Fig. 3e**, **Supplementary Fig. 3**).

To illustrate that wavelength-selectivity could be used to dynamically pattern hydrogel multimaterials, we formulated multilayered hydrogels composed of distinctly patterned regions of **Rubiq**, **Rubpy**, and *o***NB** using open-microfluidic additive manufacturing methods<sup>49</sup>. These multifunctional hydrogels were sequentially exposed to red, green, and blue light, and imaged using digital photography (**Fig. 3f**). Following red light illumination, **Rubiq** exhibited the pink-to-purple color change observed previously to accompany degradation, while **Rubpy** and *o***NB** were visibly unaltered. Treatment with green light caused **Rubpy** to lose its yellow color and degrade, leaving only *o***NB** regions intact. Final treatment with blue light yielded complete material dissolution. Exploiting conventional photolithographic methodologies, whereby homogenous gels were exposed to collimated light through a chrome photomask, patterned hydrogel degradation was achieved with high spatial resolution (**Fig. 3g**).

Encouraged by the hydrogel's rapid response to low-energy visible light, we next sought to examine whether hydrogels could be degraded through complex tissue. Skin-on pork belly was

dissected and hydrogels placed at varying depths; a **Rubiq**-crosslinked hydrogel was deposited 2 cm below the skin surface, a **Rubpy** hydrogel at 1 cm, and **oNB** (modified with Cy5-azide to enhance visualization) at 0.5 cm. Gels were respectively subjected to red, green, and blue light (50 mW cm<sup>-2</sup> at the skin) and in-tissue degradation was visually monitored (**Fig. 3h**). Hydrogel dissolution was observed for all three hydrogels following <2 hrs illumination at the depths reported. To the best of our knowledge, this is the first time that a photodegradable biomaterial has been directly controlled at these tissue depths, highlighting the potential of these materials for future in vivo applications.

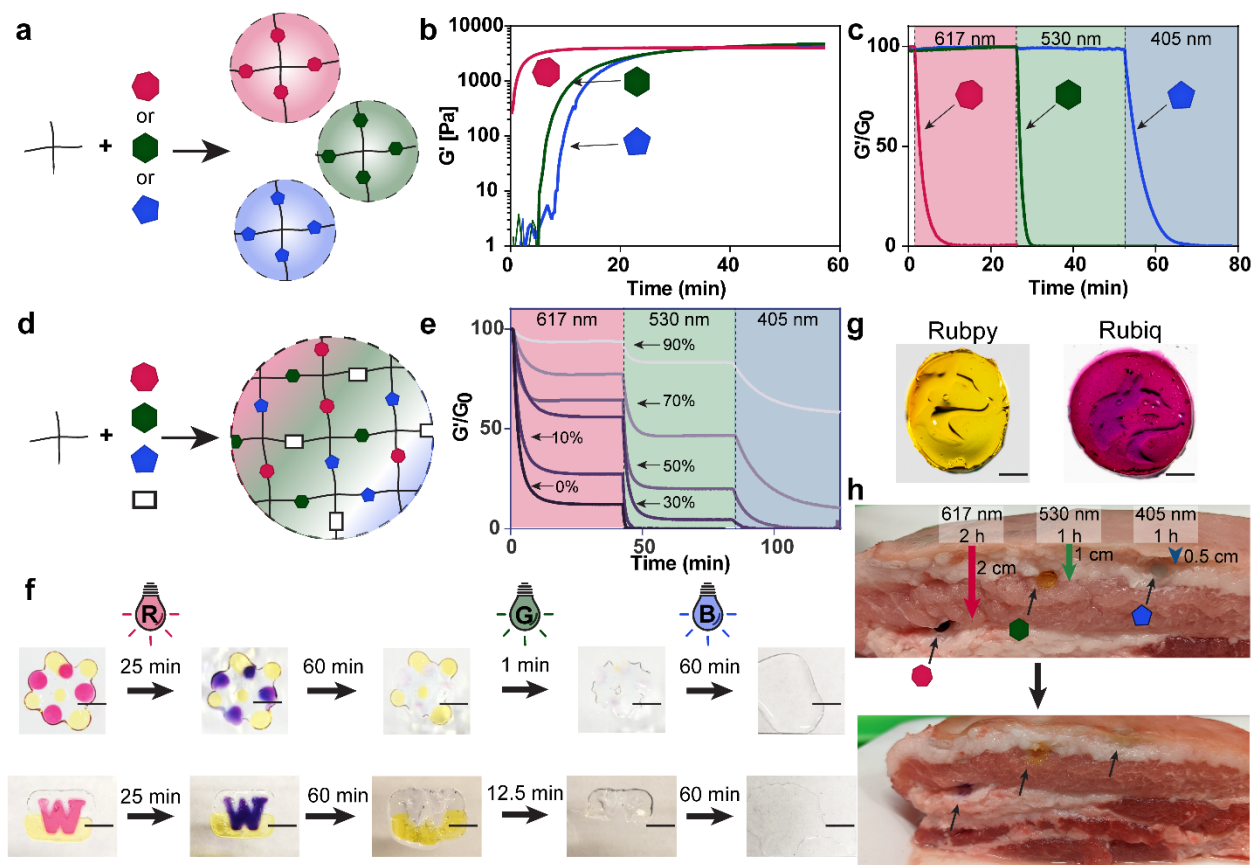


**Figure 3 | Wavelength-orthogonal hydrogel degradation via red, green, and blue light.** **a.** Hydrogels formed via SPAAC chemistry between PEG-tetraBCN and the azide-flanked crosslinkers. **b.** **Rubiq** (pink heptagon), **Rubpy** (green hexagon), and **oNB** (blue pentagon)-crosslinked hydrogels form equivalently stiff hydrogels ( $G' \sim 2\text{-}3$  kPa) as determined rheometrically. **c.** Individually crosslinked hydrogels are unidirectionally orthogonally degraded, with stable storage modulus observed in **Rubpy**-crosslinked gels under red light irradiation and

**oNB**-crosslinked gels under red and green light irradiation. **d.** Hydrogels were formed with equal ratios of all three photolabile crosslinkers and increasing amounts of nondegradable diazido-tri(ethylene glycol) (TEG) crosslinker (0 – 90%, white rectangle). **e.** Intermediate stiffnesses were accessible through partial degradation of hydrogel crosslinks. Hydrogels were exposed to red, green, then blue light (35 min each, 10 mW cm<sup>-2</sup>) to selectively cleave specific amounts of crosslinks within the material. **f.** Spatial control over hydrogel degradation demonstrated by the casting of individually crosslinked hydrogels in close proximity. Open microfluidic methodologies were used to cast interconnected multimaterial geometries; exposure to red light resulted in the center **Rubiq** degradation, with subsequent exposures to green and blue light respectively degrading the **Rubpy** and **oNB** portions. Scale bar = 5 mm. **g.** **Rubpy** and **Rubiq** hydrogels photodegraded with 530 nm light (10 mW cm<sup>-2</sup>, 5 sec) following mask-based photolithography. Scale bar = 100 μm. **h.** **Rubiq** hydrogels were completely degraded through up to 2 cm of complex tissue (skin-on pork belly shown here), **Rubpy** hydrogels through 1 cm, and **oNB** (dyed with Cy5) through 0.5 cm.

### Cell encapsulation and release from tricolor-responsive hydrogels

Having demonstrated that hydrogel responses could be controlled in a wavelength-specific manner using visible light, we next sought to investigate the cytocompatibility of gel formation via SPAAC reaction and subsequent photodegradation. 10T ½ mouse fibroblasts were encapsulated ( $5 \times 10^6$  cells mL<sup>-1</sup>) in **Rubiq**, **Rubpy**, and **oNB** hydrogels (**Fig. 4a**). Live/dead staining with calcein/ethidium homodimer and fluorescent confocal imaging was performed 24 hours after encapsulation. High viability was observed in all cases (**Fig. 4b,c**), consistent with SPAAC's reported biocompatibility for gel formation and that of the crosslinkers<sup>50</sup>. To assess the cytocompatibility of photodegradation, cell-laden gels were photodegraded with red, green, or blue visible light 1 day post encapsulation. In a subset of the gels, released cells were left suspended in hydrogel photoproducts for an additional 24 hours, after which the cells that adhered were stained for viability (**Fig. 4c**). Fibroblasts showed normal morphology 24 hours after plating, suggesting the photodegradation process did not alter them significantly. To confirm viability following release, cells were collected following hydrogel degradation and assessed directly for viability via flow cytometry (**Fig. 4d**). Though viability was generally high,

results demonstrated that fibroblasts released from **Rubiq**-crosslinked gels were less viable than the other hydrogel formulations, suggesting that the **Rubiq** photoproduct may be partially cytotoxic.

Taking advantage of the spatial resolution afforded by this hydrogel system using orthogonal wavelengths of light, unique cell populations were encapsulated and recovered from individual hydrogels. Human bone marrow-derived stromal cells (hS5) stably expressing either mCherry, GFP, or BFP were encapsulated in **Rubiq**, **Rubpy**, and **oNB**-crosslinked hydrogels, respectively (**Fig. 4e**). Upon irradiation with red, green, or blue light, selective hydrogel degradation was observed by confocal microscopy (**Fig. 4f**). Following degradation, the gel-liberated cell populations were collected and analyzed via flow cytometry. Harvested cell collections matched the expected color composition: 617 nm light released only mCherry<sup>+</sup> cells, 530 nm yielded matched populations of mCherry<sup>+</sup> and GFP<sup>+</sup>, and 405 nm light degraded all three hydrogels and gave equivalent counts of mCherry<sup>+</sup>, GFP<sup>+</sup>, and BFP<sup>+</sup> cells (**Fig. 4g**). Results further demonstrate wavelength orthogonality and multiplexability of cell release from tricolor visible light-responsive gels.

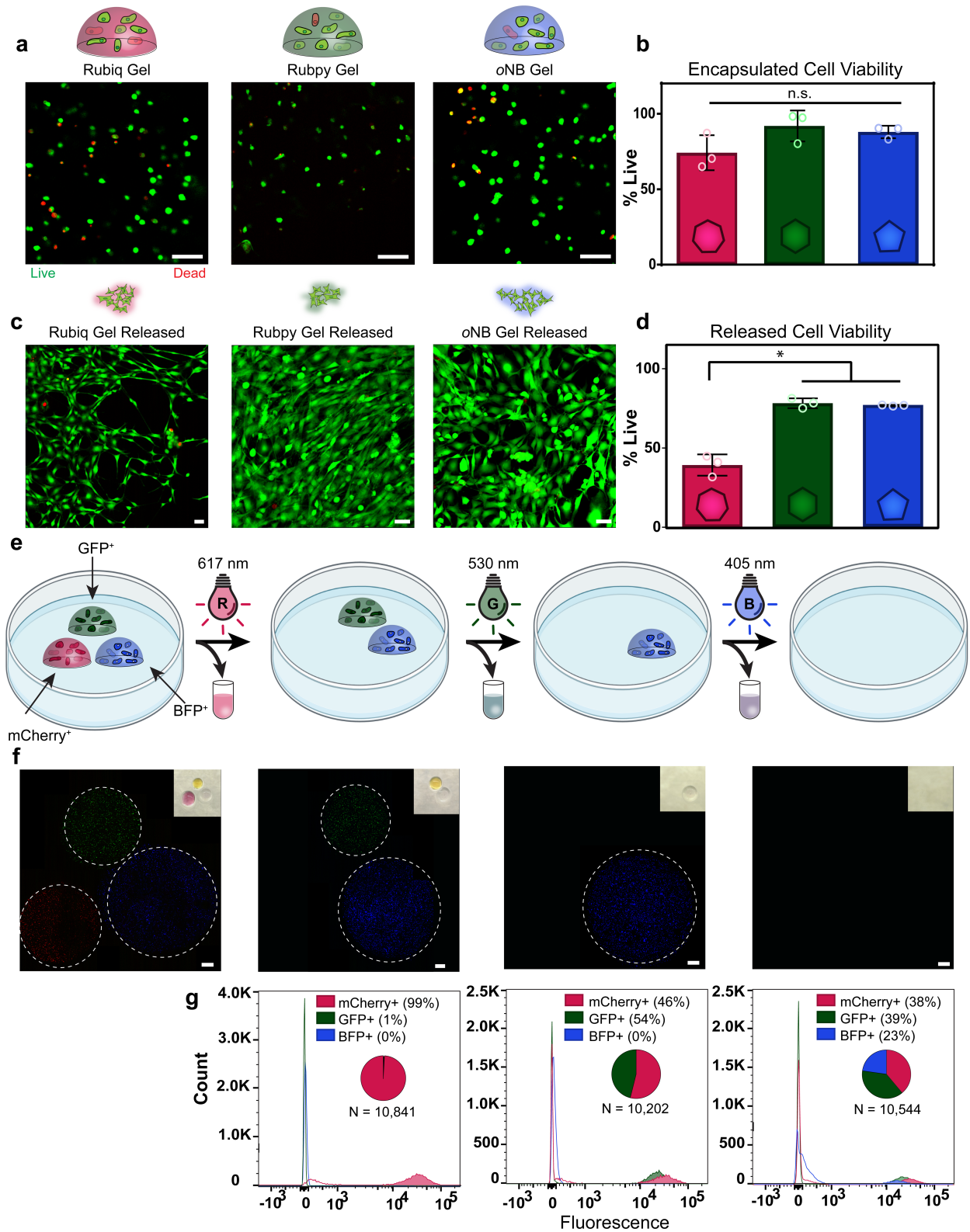


**Figure 4 | Cell viability following encapsulation and photorelease in Rubiq, Rubpy, and oNB-crosslinked hydrogels.** a. Live/dead staining of 10T  $\frac{1}{2}$  fibroblasts encapsulated in and released from individually crosslinked hydrogels. Calcein (green) and ethidium homodimer

(EtHD, red) dyes were used for live and dead staining respectively. Scale bar = 50  $\mu\text{m}$ . **b.** Encapsulated cell viability at 24 hours post encapsulation. Cell counting revealed no statistical difference in cell viability across all crosslinkers at 24 hours. **c. Rubiq, Rubpy, and oNB** hydrogels were exposed to red, green, or blue light respectively (617 nm, 530 nm, 405 nm; 10  $\text{mW cm}^{-2}$ ) and the released fibroblasts allowed to settle to the bottom of the well over 24 hr prior to imaging. Surviving cells exhibited classical fibroblast morphology upon calcein green/EtHD staining. Scale bars = 50  $\mu\text{m}$ . **d.** High levels of viable cells were recovered from each hydrogel formulation, though cells released from **Rubiq** hydrogels showed lower levels of viability compared to **Rubpy** and **oNB**. \*\*  $p < 0.0036$  **e.** hS5-mCherry<sup>+</sup>, hS5-GFP<sup>+</sup>, and hS5-BFP<sup>+</sup> cells were encapsulated in **Rubiq, Rubpy, and oNB** hydrogels respectively. 24 hours after encapsulation, hydrogels were exposed to 617 nm, 530 nm, or 405 nm light. **f.** Images of hydrogels bearing mCherry<sup>+</sup>, GFP<sup>+</sup>, or BFP<sup>+</sup> hS5 cells following light exposure. Scale bars = 500  $\mu\text{m}$ . **g.** Flow cytometry histograms show only expected cell populations were released into the media, demonstrating the orthogonality of the hydrogel system.

## **Discussion:**

In summary, novel crosslinkers **Rubiq**, **Rubpy**, and **oNB** provide a route towards the first tricolor visible light-degradable gel system. We have established that these crosslinkers are synthetically accessible with moderate yields and photoresponsive to low-energy light. These species are highly photoactive under visible light irradiation rendering PEG-based hydrogels that rapidly and orthogonally degrade under red (617 nm), green (530 nm) and blue (405 nm) light. The use of low-energy light permits hydrogel degradation through complex tissue up to 2 cm in depth, while wavelength-orthogonality enables sequential and spatial control over hydrogel degradation. We have demonstrated crosslinker cytocompatibility, with encapsulated cell viability  $\geq 85\%$  for all hydrogels over the lifetime of the hydrogel in tissue culture conditions. Exploiting their wavelength-selective degradation, we demonstrated multiplexed cell populations recovery, a feature that is likely to be useful for in vivo cell delivery applications. Moving forward, we anticipate that these materials will prove enabling for additional applications in mechanobiology, 4D cell culture, and controlled therapeutic release.

## **Methods:**

**General synthetic methods.** All reactions and purification protocols were performed under red light. All solvents and chemicals were used as received with no further purification.

### **4-azidobutyronitrile**

4-bromobutyronitrile (1 mL, 10 mmol) and sodium azide (1.3 g, 20 mmol) were dissolved in dimethylsulfoxide (DMSO, 15 mL) and stirred overnight at 55 °C. The reaction was cooled to room temperature, diluted with water to 50 mL, extracted with diethyl ether (3x 50 mL), dried over Na<sub>2</sub>SO<sub>4</sub>, and the ether was removed under vacuum to give the product as a light-yellow oil. Yield: 1.017 g, 92%. <sup>1</sup>H NMR: (CDCl<sub>3</sub>, 300 MHz) δ 3.50 (t, 2H, *J*=6.34), 2.48 (t, 2H, *J*=7.05), 1.92 (quint, 2H, *J*=12.96).

### **Ru(biquinoline)<sub>2</sub>Cl<sub>2</sub> (Ru(biq)<sub>2</sub>Cl<sub>2</sub>)**

RuCl<sub>3</sub> (anhydrous, 99.96% trace metal basis, 400 mg, 1.93 mmol), hydroquinone (444 mg, 4 mmol), and LiCl (480 mg, 11.3 mmol) were suspended in dimethylformamide (DMF, 10 mL) and bubbled with N<sub>2</sub> for 15 min. Reaction was heated to 130 °C for 1 h until color appeared forest green, then cooled to room temperature. Reaction was added dropwise to 800 mL deionized water and filtered to collect a dark green-black solid. Solid was dissolved in dichloromethane (200 mL), solvent was reduced to 100 mL under vacuum, then added to diethyl ether (400 mL) and filtered to collect Ru(biq)<sub>2</sub>Cl<sub>2</sub> as a dark green solid. Product was used without further purification. Yield: 805 mg, 61%.

### **Ru(biq)<sub>2</sub>(4-azidobutyronitrile)<sub>2</sub>[Cl<sub>2</sub>] (Rubiq)**

Ru(biq)<sub>2</sub>Cl<sub>2</sub> (250 mg, 0.365 mmol) and silver hexafluorophosphate (275 mg, 1.08 mmol) were dissolved in methanol (40 mL, stored over molecular sieves) and stirred at 55 °C in the dark until reaction turned blue and white silver chloride powder was observed (15 min). 4-azidobutyronitrile (100 μL, 0.945 mmol) was added, and reaction stirred at 55 °C for 1 hour until color turned pink. Reaction was cooled to room temperature, filtered to remove silver chloride, and methanol was removed by rotary evaporation. Ru(biq)<sub>2</sub>(4-azidobutyronitrile)<sub>2</sub> was purified by silica flash chromatography with 1:4 acetonitrile:dichloromethane as the eluent.

Ru(biq)<sub>2</sub>(4-azidobutyronitrile)<sub>2</sub>[PF<sub>6</sub>]<sub>2</sub> was converted to the chloride salt by anion-exchange resin. RuPink[PF<sub>6</sub>]<sub>2</sub> was passed over Amberlite IRA-410 (Cl Form) resin using methanol as the eluent, giving Ru(biq)<sub>2</sub>(4-azidobutyronitrile)<sub>2</sub>[Cl]<sub>2</sub> as the water-soluble form (denoted **Rubiq**). Yield: 159 mg, 48%. Overall yield: 27% <sup>1</sup>H NMR: (CD<sub>3</sub>CN, 300 MHz) δ 9.14 (broad s, 2H), 8.68 (d, 2H, *J*=8.69), 8.36 (d, 2H, *J*=7.99), 8.31 (d, 2H, *J*=8.09), 8.21 (broad s, 2H), 8.02 (t, 2H, *J*=7.27), 7.91 (d, 2H, *J*=7.84), 7.50 (t, 2H, *J*=7.04), 6.87 (t, 2H, *J*=7.17), 6.75 (d, 2H, *J*=8.4), 3.08 (t, 4H, *J*=6.42), 2.75 (t, 4H, *J*=7.25), 1.65 (quint, 4H, *J*=6.57). Expected mass [H<sup>+</sup>, m/2]: 417.11, observed mass: 417.1125 (m/2).

*Ru(bpy)<sub>2</sub>(4-azidobutyronitrile)<sub>2</sub>[Cl]<sub>2</sub>* (**Rubpy**)

Ru(bipyridine)<sub>2</sub>Cl<sub>2</sub>•2H<sub>2</sub>O (200 mg, 0.38 mmol) and silver hexafluorophosphate (212 mg, 0.83 mmol) were dissolved in methanol (stored over molecular sieves, 40 mL) and stirred at 55 °C for 15 minutes. 4-azidobutyronitrile (390 μL, 3.7 mmol) was added and the reaction stirred at 55 °C for 2 hours until color changed from red to orange. Reaction mixture was cooled to room temperature and filtered to remove silver chloride, then concentrated by rotary evaporation. The

product (denoted **Rubpy**) was purified by silica flash chromatography with 4:1 dichloromethane:acetonitrile as the eluent, collecting the major yellow band. Yield: 22 mg, 84%. Overall yield: 77% <sup>1</sup>H NMR: (CD<sub>3</sub>CN, 300 MHz) δ 9.61 (d, 2H, *J*=4.95), 8.83 (d, 2H, *J*=8.07), 8.69 (d, 2H, *J*=8.10), 8.43 (t, 2H, *J*=7.16), 8.12 (t, 2H, *J*=7.16), 8.00 (t, 2H, *J*=6.00), 7.93 (d, 2H, *J*=5.70), 7.46 (t, 2H, *J*=6.00), 3.37 (t, 4H, *J*=6.33), 3.00 (t, 4H, *J*=6.74), 1.90 (quint, 4H, *J*=6.58). Expected mass (m/2):

#### 4-azidobutanoic acid (N<sub>3</sub>-COOH)

N<sub>3</sub>-COOH was synthesized based on published procedures and used with minor modifications<sup>44</sup>. Ethyl-4-bromobutyrate (36.6 mL, 254 mmol) and sodium azide (25 g, 380 mmol) were dissolved in DMSO (375 mL) and reacted at 55 °C overnight. The reaction was cooled to room temperature and diluted with water (250 mL) and extracted with diethyl ether (3x100 mL). The organic layer was washed with brine (250 mL) and dried over Na<sub>2</sub>SO<sub>4</sub>, and concentrated by rotary evaporator to give the intermediate ethyl-4-azidobutanoate as a yellow oil. Yield: 32.5 g, 80%.

Ethyl-4-azidobutanoate (32.5 g, 0.205 mmol) was dissolved in 150 mL of methanol. 1M sodium hydroxide (aqueous, 250 mL) was added and the mixture was stirred at room temperature for 3 hours. Methanol (~75 mL) was partially removed by rotary evaporation and concentrated hydrochloric acid (HCl) was added until the pH reached 1. The product was extracted into diethyl ether (3 x 250 mL), dried over Na<sub>2</sub>SO<sub>4</sub>, and the ether was removed to give 4-azidobutanoic acid as a yellow oil. Yield: 27 g, 84%. <sup>1</sup>H NMR (CDCl<sub>3</sub>, 300 MHz) 6.29 (br s, 1H), 3.51 (q, 2H, *J*=7.04), 3.37 (t, 2H, *J*=6.72), 2.45 (quint, 2H, *J*=7.23), 1.21 (t, 2H, *J*=7.03)

4-(4-(1-((4-azidobutanoyl)oxy)ethyl)-2-methoxy-5-nitrophenoxy)butanoic acid (N<sub>3</sub>-oNB-COOH)

N<sub>3</sub>-COOH (27 g, 209 mmol) and N,N'-Dicyclohexylcarbodiimide (DCC, 13.8 g, 67 mmol) were mixed under nitrogen in a flame-dried flask. Dry dichloromethane (DCM, 170 mL) was added and the reaction stirred at room temperature for 1 hour. Solid urea byproduct was filtered over glass frit and the reaction mixture concentrated by rotary evaporation (filtration step repeated if more byproduct precipitate was observed).

HO-oNB-COOH (4-(4-(1-hydroxyethyl)-2-methoxy-5-nitrophenoxy)butanoic acid, 4.2 g, 14 mmol) and 4-dimethylaminopyridine (DMAP, 86 mg, 0.7 mmol) were mixed with the crude anhydride and dissolved in minimal dichloromethane (DCM, 100 mL). Pyridine (1.13 mL, 14 mmol) was added and reaction was stirred under nitrogen overnight until color turned dark brown. Reaction was washed with saturated sodium bicarbonate (NaHCO<sub>3</sub>, 250 mL) and 1M aqueous HCl and concentrated by rotary evaporation. Reaction was dissolved in 1:1 water:acetone (500 mL) and stirred overnight at room temperature.

Acetone was removed by rotary evaporation and product extracted into dichloromethane (3 x 250 mL). The organic layer was washed with 1M HCl, dried over sodium sulfate and concentrated. Product was purified by flash silica column chromatography, 20-40% ethyl acetate in hexanes with 1% acetic acid, product eluted as trailing yellow band giving N<sub>3</sub>-oNB-COOH as a yellow oil. Yield: 4.3 g, 71%. <sup>1</sup>H NMR (CDCl<sub>3</sub>, 300 MHz) δ 7.57 (s, 1H), 7.10 (s, 1H), 6.21 (q, 1H, *J*=6.44), 4.08 (t, 2H, *J*=6.47), 3.96 (s, 3H), 3.32 (t, 2H, *J*=6.84), 2.43 (t, 2H, *J*=6.21), 2.38 (t, 2H, *J*=6.34), 1.96 (quint, 2H, *J*=6.91), 1.76 (t, 2H, *J*=6.98), 1.58 (d, 3H, *J*=6.54).

1-(4-(4-((2-(2-(2-azidoethoxy)ethoxy)ethyl)amino)-4-oxobutoxy)-5-methoxy-2-nitrophenyl)ethyl

4-azidobutanoate (oNB)

N<sub>3</sub>-oNB-COOH (2.1 g, 5 mmol), 1-[Bis(dimethylamino)methylene]-1H-1,2,3-triazolo[4,5-b]pyridinium 3-oxid hexafluorophosphate (HATU, 950 mg, 2.5 mmol), and diisopropylamine (DIEA, 3.56 mL, 20 mmol) were dissolved in DMF and stirred for 20 min to prereact. N<sub>3</sub>-TEG-NH<sub>2</sub> (741 μL, 5.1 mmol) was added and the reaction stirred at room temperature for 90 min. The reaction mixture was diluted with ethyl acetate (300 mL), washed with water (3 x 100 mL), dried over magnesium sulfate, and concentrated by rotary evaporation. Product (denoted oNB) was purified by silica flash chromatography, 2:1 ethyl acetate:hexanes; collected the last yellow band. Yield: 849 mg, 30%. Overall yield: 18% <sup>1</sup>H NMR: (CDCl<sub>3</sub>, 300 MHz) δ 7.55 (s, 1H), 7.00 (s, 1H), 6.45 (q, 1H, *J*=6.35), 6.27 (brd t, 1H), 4.07 (t, 2H, *J*=5.43), 3.95 (s, 3H), 3.66 (t, 2H, *J*=4.92), 3.62 (s, 4H), 3.54 (t, 2H, *J*=5.09), 3.44 (p, 2H, *J*=5.22), 3.37 (t, 2H, *J*=4.86), 3.31 (t, 2H, *J*=6.63), 2.47-2.37 (m, 4H), 2.17 (t, 2H, *J*=6.69), 1.87 (q, 2H, *J*=9.15), 1.60 (d, 3H, *J*=6.39). Expected Mass: [+H] 567.25, observed 567.21.

PEG-tetraBCN

Following previously published protocol<sup>44</sup>, PEG-tetraamine (M<sub>n</sub> ~ 20 kDa, 4-arm, 1.13 g, 0.0571 mmol) and BCN-OSu (100 mg, 0.343 mmol) were added to a flame-dried scintillation vial under nitrogen. Anhydrous DMF (5 mL) and DIEA (159 uL, 4x) was added and the reaction was stirred under nitrogen overnight at room temperature. Water (50 mL) was added to the reaction mixture which was then dialyzed in SpectraPor dialysis tubing (3k MWCO) overnight at 4 °C.

The PEG-tetraBCN was recovered as a powder by lyophilization and resuspended at 10 mM in PBS for gel formation.

**Quantum yield determination.** The quantum yield of photocleavage was determined via kinetic analysis of the cleavage reaction as observed by UV-Vis spectrometry<sup>51</sup>. In brief, the absorbance at a given wavelength for each crosslinker (550 nm for Ru(biq)<sub>2</sub>, 445 nm for Ru(bpy)<sub>2</sub>, and 375 nm for oNB) was tracked as each sample was exposed to light. The data were fit to an equation of the form:

$$y = A_1 e^{-x/\tau_1} + A_2 e^{-x/\tau_2} + y_0$$

with two time constants  $\tau_1$  and  $\tau_2$  that give rate constants  $k_1$  and  $k_2$  according to

$$k_1 = -\frac{1}{\tau_1}, k_2 = -\frac{1}{\tau_2}$$

The quantum yield ( $\Phi$ ) was extracted from the rate constant for each crosslinker according to

$$\Phi = \frac{k_1 [A]_i V_{sample}}{\frac{P}{E_{ph} N_A}}$$

Where:

$k_1$  is the rate constant for photolysis

$[A]_i$  is the initial concentration of the crosslinker

$V_{sample}$  is the total volume of the sample irradiated

$P$  is the power of the incoming light, measured in Watts ( $J \text{ sec}^{-1}$ )

$E_{ph}$  is the energy of the photon, given by  $\frac{hc}{\lambda}$ , where  $h$  is Plank's constant,  $c$  is the speed of light in a vacuum, and  $\lambda$  is the wavelength of incident light

$N_A$  is Avogadro's number

**Hydrogel formation.** Hydrogels were formed via SPAAC by mixing of PEG-tetraBCN (final concentration of 3 mM) with the diazide crosslinkers (final concentration of 6 mM). For

hydrogels used in cell culture, an azide-modified RGD peptide (N<sub>3</sub>-GRGD<sub>2</sub>-NH<sub>2</sub>) was included (final concentration of 1 mM).

**Rheometric characterization of hydrogel viscoelasticity.** Hydrogels were formed on the rheometer (20  $\mu$ L, working distance = 0.3 mm) and gelation was observed in a timesweep experiment (angular frequency = 6.28 rad s<sup>-1</sup>). Following complete hydrogel formation as indicated by storage modulus plateau, gels were swelled in 0.1 mM NaN<sub>3</sub> to cap any remaining BCN groups prior to photodegradation. Hydrogels were exposed to light via a quartz bottom plate coupled to a fiber optic light guide from a multiwavelength LED light source.

**Cell encapsulation and viability studies.** Trypsinized 10 T  $\frac{1}{2}$  mouse fibroblasts were encapsulated in SPAAC hydrogels at 5 x 10<sup>6</sup> cells mL<sup>-1</sup> via direct mixing with hydrogel precursors. Hydrogels were formed and incubated at 37 °C and 5% CO<sub>2</sub> for 30 minutes before being submerged in DMEM.

Cell viability was assayed by live/dead staining with calcein green and ethidium homodimer (EtHD), respectively. Hydrogels were washed in PBS and incubated in live/dead staining solution (4  $\mu$ M EtHD, 2  $\mu$ M calcein) for 1 hour prior to confocal imaging. Live/dead cell count was quantified from max intensity projections spanning 50  $\mu$ m of hydrogel using CellProfiler and normalized to cell viability in TEG-crosslinked hydrogels.

For flow cytometry viability assays, cell-laden hydrogels were degraded using the appropriate wavelength of light, cells were collected and pelleted, and resuspended in calcein/EtHD solution for 15 minutes before counting.

**Photorelease of human stromal cells from gels for flow cytometry.** hS5 stromal cells stably expressing BFP, GFP, and mCherry were encapsulated in PEG-tetraBCN hydrogels crosslinked with the appropriate photocleavable crosslinker (RuPink with hS5-mCherry<sup>+</sup>, RuOrange with hS5-GFP<sup>+</sup>, and *o*NB with hS5-BFP<sup>+</sup>). All three hydrogels were cast in the same tissue culture dish, allowed to form for 30 minutes, then incubated in RPMI media for 24 hours.

Hydrogels were transferred to PBS and exposed to 617 nm, 530 nm, or 405 nm light (10 mW cm<sup>-2</sup>, until hydrogel degradation was observed) and the resulting cell suspension was collected and analyzed by flow cytometry. Any hydrogels left intact after irradiation were imaged using confocal fluorescent microscopy.

**Acknowledgements:**

The authors would like to acknowledge R. Bretherton and I. Kopyeva for helpful suggestions related to cell culture. This work was supported by a CAREER Award (DMR 1652141, C.A.D.) and grants (DMR 1807398, C.A.D.) from the National Science Foundation, as well as a Maximizing Investigators' Research Award (R35GM138036, C.A.D.) from the National Institutes of Health. Postdoctoral fellowship support was provided by the Washington Research Foundation (to T.L.R.). Part of this work was conducted with instrumentation provided by the Joint Center for Deployment and Research in Earth Abundant Materials (JCDREAM).

**Author contributions:**

For this manuscript, T.L.R. and C.A.D. conceived and designed the experiments; T.L.R. performed the experiments and analyzed the data; T.L.R. and C.A.D. prepared the figures; T.L.R. and C.A.D. wrote the paper.

**Competing financial interests:**

The authors declare no competing financial interests.

**Availability of Data and Materials:**

All pertinent experimental procedures, materials, methods, and characterization data are available within this manuscript and its associated Supplementary Information.

## **References:**

1. Ruskowitz, E. R. & DeForest, C. A. Photoresponsive biomaterials for targeted drug delivery and 4D cell culture. *Nat. Rev. Mater.* **3**, 17087 (2018).
2. Rapp, T. L. & DeForest, C. A. Visible Light-Responsive Dynamic Biomaterials: Going Deeper and Triggering More. *Adv. Healthc. Mater.* **9**, 1901553 (2020).
3. Rapp, T. L. & DeForest, C. A. Targeting drug delivery with light: A highly focused approach. *Adv. Drug Deliv. Rev.* **171**, (2021).
4. Munoz-Robles, B. G., Kopyeva, I. & DeForest, C. A. Surface Patterning of Hydrogel Biomaterials to Probe and Direct Cell–Matrix Interactions. *Adv. Mater. Interfaces* **7**, 2001198 (2020).
5. Gilbert, P. M., Havenstrite, K. L., Magnusson, K. E. G., Sacco, A., Leonardi, N. A., Kraft, P., Nguyen, N. K., Thrun, S., Lutolf, M. P. & Blau, H. M. Substrate Elasticity Regulates Skeletal Muscle Stem Cell Self-Renewal in Culture. *Science* **329**, 1078–1081 (2010).
6. Hofer, M. & Lutolf, M. P. Engineering organoids. *Nat. Rev. Mater.* **2021 65** **6**, 402–420 (2021).
7. Tibbitt, M. W. & Anseth, K. S. Hydrogels as Extracellular Matrix Mimics for 3D Cell Culture. *Biotechnol. Bioeng.* **103**, 655–663 (2009).
8. Yang, C., Tibbitt, M. W., Basta, L. & Anseth, K. S. Mechanical memory and dosing influence stem cell fate. *Nat. Mater.* **2014 136** **13**, 645–652 (2014).
9. Elosegui-Artola, A., Gupta, A., Najibi, A. J., Seo, B. R., Garry, R., Darnell, M., Gu, W., Zhou, Q., Weitz, D. A., Mahadevan, L., Mooney, D. J., John, -Harvard & Paulson, A. Matrix viscoelasticity controls spatio-temporal tissue organization. *bioRxiv* 2022.01.19.476771 (2022). doi:10.1101/2022.01.19.476771

10. Below, C. R., Kelly, J., Brown, A., Humphries, J. D., Hutton, C., Xu, J., Lee, B. Y., Cintas, C., Zhang, X., Hernandez-Gordillo, V., Stockdale, L., Goldsworthy, M. A., Geraghty, J., Foster, L., O'Reilly, D. A., Schedding, B., Askari, J., Burns, J., Hodson, N., Smith, D. L., Lally, C., Ashton, G., Knight, D., Mironov, A., Banyard, A., Eble, J. A., Morton, J. P., Humphries, M. J., Griffith, L. G. & Jørgensen, C. A microenvironment-inspired synthetic three-dimensional model for pancreatic ductal adenocarcinoma organoids. *Nat. Mater.* 2021 211 **21**, 110–119 (2021).
11. Fang, Y. & Eglén, R. M. Three-Dimensional Cell Cultures in Drug Discovery and Development. *SLAS Discov.* **22**, 456–472 (2017).
12. Antonica, F., Kasprzyk, D. F., Opitz, R., Iacovino, M., Liao, X. H., Dumitrescu, A. M., Refetoff, S., Peremans, K., Manto, M., Kyba, M. & Costagliola, S. Generation of functional thyroid from embryonic stem cells. *Nat.* 2012 4917422 **491**, 66–71 (2012).
13. Huch, M., Dorrell, C., Boj, S. F., Van Es, J. H., Li, V. S. W., Van De Wetering, M., Sato, T., Hamer, K., Sasaki, N., Finegold, M. J., Haft, A., Vries, R. G., Grompe, M. & Clevers, H. In vitro expansion of single Lgr5<sup>+</sup> liver stem cells induced by Wnt-driven regeneration. *Nat.* 2013 4947436 **494**, 247–250 (2013).
14. Lancaster, M. A., Renner, M., Martin, C. A., Wenzel, D., Bicknell, L. S., Hurles, M. E., Homfray, T., Penninger, J. M., Jackson, A. P. & Knoblich, J. A. Cerebral organoids model human brain development and microcephaly. *Nat.* 2013 5017467 **501**, 373–379 (2013).
15. Mateen, R., Ali, M. M. & Hoare, T. A printable hydrogel microarray for drug screening avoids false positives associated with promiscuous aggregating inhibitors. *Nat. Commun.* 2018 91 **9**, 1–9 (2018).
16. DeForest, C. A. & Tirrell, D. A. A photoreversible protein-patterning approach for

- guiding stem cell fate in three-dimensional gels. *Nat. Mater.* **14**, 523–531 (2015).
17. Kirschner, C. M., Alge, D. L., Gould, S. T. & Anseth, K. S. Clickable, Photodegradable Hydrogels to Dynamically Modulate Valvular Interstitial Cell Phenotype. *Adv. Healthc. Mater.* **3**, 649–657 (2014).
  18. Gjorevski, N., Nikolaev, M., Brown, T. E., Mitrofanova, O., Brandenburg, N., DelRio, F. W., Yavitt, F. M., Liberali, P., Anseth, K. S. & Lutolf, M. P. Tissue geometry drives deterministic organoid patterning. *Science* **375**, (2022).
  19. Yavitt, F. M., Kirkpatrick, B. E., Blatchley, M. R. & Anseth, K. S. 4D Materials with Photoadaptable Properties Instruct and Enhance Intestinal Organoid Development. *ACS Biomater. Sci. Eng.* (2022). doi:10.1021/acsbiomaterials.1c01450
  20. Killaars, A. R., Grim, J. C., Walker, C. J., Hushka, E. A., Brown, T. E. & Anseth, K. S. Extended Exposure to Stiff Microenvironments Leads to Persistent Chromatin Remodeling in Human Mesenchymal Stem Cells. *Adv. Sci.* **6**, 1801483 (2019).
  21. Walker, C. J., Crocini, C., Ramirez, D., Killaars, A. R., Grim, J. C., Aguado, B. A., Clark, K., Allen, M. A., Dowell, R. D., Leinwand, L. A. & Anseth, K. S. Nuclear mechanosensing drives chromatin remodelling in persistently activated fibroblasts. *Nat. Biomed. Eng.* **2021 512** **5**, 1485–1499 (2021).
  22. Shadish, J. A., Benuska, G. M. & DeForest, C. A. Bioactive site-specifically modified proteins for 4D patterning of gel biomaterials. *Nat. Mater.* **18**, 1005–1014 (2019).
  23. Batalov, I., Stevens, K. R. & DeForest, C. A. Photopatterned biomolecule immobilization to guide three-dimensional cell fate in natural protein-based hydrogels. *Proc. Natl. Acad. Sci.* **118**, e2014194118 (2021).
  24. Cai, Z., Huang, K., Bao, C., Wang, X., Sun, X., Xia, H., Lin, Q., Yang, Y. & Zhu, L.

- Precise Construction of Cell-Instructive 3D Microenvironments by Photopatterning a Biodegradable Hydrogel. *Chem. Mater.* **31**, 4710–4719 (2019).
25. Headen, D. M., Woodward, K. B., Coronel, M. M., Shrestha, P., Weaver, J. D., Zhao, H., Tan, M., Hunckler, M. D., Bowen, W. S., Johnson, C. T., Shea, L., Yolcu, E. S., García, A. J. & Shirwan, H. Local immunomodulation with Fas ligand-engineered biomaterials achieves allogeneic islet graft acceptance. *Nat. Mater.* **17**, 732–739 (2018).
  26. Azagarsamy, M. A., McKinnon, D. D., Alge, D. L. & Anseth, K. S. Coumarin-Based Photodegradable Hydrogel: Design, Synthesis, Gelation, and Degradation Kinetics. *ACS Macro Lett.* **3**, 515–519 (2014).
  27. Azagarsamy, M. A. & Anseth, K. S. Wavelength-Controlled Photocleavage for the Orthogonal and Sequential Release of Multiple Proteins. *Angew. Chemie Int. Ed.* **52**, 13803–13807 (2013).
  28. Pelloth, J. L., Tran, P. A., Walther, A., Goldmann, A. S., Frisch, H., Truong, V. X. & Barner-Kowollik, C. Wavelength-Selective Softening of Hydrogel Networks. *Adv. Mater.* **33**, 2102184 (2021).
  29. Jacques, S. L. Optical properties of biological tissues: A review. *Physics in Medicine and Biology* **58**, R37 (2013).
  30. Rapp, T. L., Wang, Y., Delessio, M. A., Gau, M. R. & Dmochowski, I. J. Designing photolabile ruthenium polypyridyl crosslinkers for hydrogel formation and multiplexed, visible-light degradation. *RSC Adv.* **9**, (2019).
  31. Griffin, D. R. & Kasko, A. M. Photodegradable macromers and hydrogels for live cell encapsulation and release. *J. Am. Chem. Soc.* **134**, 13103–7 (2012).
  32. Menzel, J. P., Feist, F., Tuten, B., Weil, T., Blinco, J. P. & Barner-Kowollik, C. Light-

- Controlled Orthogonal Covalent Bond Formation at Two Different Wavelengths. *Angew. Chemie Int. Ed.* **58**, 7470–7474 (2019).
33. Truong, V. X., Bachmann, J., Unterreiner, A., Blinco, J. P. & Barner-Kowollik, C. Wavelength-Orthogonal Stiffening of Hydrogel Networks with Visible Light. *Angew. Chemie Int. Ed.* **61**, e202113076 (2022).
34. Zayat, L., Calero, C., Alborés, P., Baraldo, L. & Etchenique, R. A new strategy for neurochemical photodelivery: metal-ligand heterolytic cleavage. *J. Am. Chem. Soc.* **125**, 882–3 (2003).
35. Li, A., Turro, C. & Kodanko, J. J. Ru(II) polypyridyl complexes as photocages for bioactive compounds containing nitriles and aromatic heterocycles. *Chem. Commun.* **54**, 1280–1290 (2018).
36. Griepenburg, J. C., Rapp, T. L., Carroll, P. J., Eberwine, J. & Dmochowski, I. J. Ruthenium-caged antisense morpholinos for regulating gene expression in zebrafish embryos. *Chem. Sci.* **6**, 2342–2346 (2015).
37. Rapp, T. L., Highley, C. B., Manor, B. C., Burdick, J. A. & Dmochowski, I. J. Ruthenium-Crosslinked Hydrogels with Rapid, Visible-Light Degradation. *Chem. - A Eur. J.* **24**, 2328–2333 (2018).
38. Rapp, T. L., Wang, Y., Delessio, M. A., Gau, M. R. & Dmochowski, I. J. Designing photolabile ruthenium polypyridyl crosslinkers for hydrogel formation and multiplexed, visible-light degradation. *RSC Adv.* **9**, 4942–4947 (2019).
39. Arora, K., Herroon, M., Al-Afyouni, M. H., Toupin, N. P., Rohrabough, T. N., Loftus, L. M., Podgorski, I., Turro, C. & Kodanko, J. J. Catch and Release Photosensitizers: Combining Dual-Action Ruthenium Complexes with Protease Inactivation for Targeting

- Invasive Cancers. *J. Am. Chem. Soc.* **140**, 14367–14380 (2018).
40. Havrylyuk, D., Hachey, A. C., Fenton, A., Heidary, D. K. & Glazer, E. C. Ru(II) photocages enable precise control over enzyme activity with red light. *Nat. Commun.* **2022 131** **13**, 1–10 (2022).
  41. Sun, W., Li, S., Häupler, B., Liu, J., Jin, S., Steffen, W., Schubert, U. S., Butt, H.-J., Liang, X.-J. & Wu, S. An Amphiphilic Ruthenium Polymetallodrug for Combined Photodynamic Therapy and Photochemotherapy In Vivo. *Adv. Mater.* **29**, 1603702 (2017).
  42. Al-Afyouni, M. H., Rohrabough, T. N., Al-Afyouni, K. F. & Turro, C. New Ru(II) photocages operative with near-IR light: new platform for drug delivery in the PDT window. *Chem. Sci.* **9**, 6711–6720 (2018).
  43. Havrylyuk, D., Stevens, K., Parkin, S. & Glazer, E. C. Toward Optimal Ru(II) Photocages: Balancing Photochemistry, Stability, and Biocompatibility Through Fine Tuning of Steric, Electronic, and Physiochemical Features. *Inorg. Chem.* **59**, 1006–1013 (2020).
  44. Badeau, B. A., Comerford, M. P., Arakawa, C. K., Shadish, J. A. & DeForest, C. A. Engineered modular biomaterial logic gates for environmentally triggered therapeutic delivery. *Nat. Chem.* **10**, 251–258 (2018).
  45. Agard, N. J., Prescher, J. A. & Bertozzi, C. R. A strain-promoted [3 + 2] azide-alkyne cycloaddition for covalent modification of biomolecules in living systems. *J. Am. Chem. Soc.* **126**, 15046–15047 (2004).
  46. Dixon, I. M., Bonnet, S., Alary, F. & Cuny, J. Photoinduced Ligand Exchange Dynamics of a Polypyridyl Ruthenium Complex in Aqueous Solution. *J. Phys. Chem. Lett.* **12**, 7278–7284 (2021).

47. Loftus, M., Al-Afyouni, D. & Turro, C. New Ru II Scaffold for Photoinduced Ligand Release with Red Light in the Photodynamic Therapy (PDT) Window. *Chem. Eur.J* **24**, 11550–11553 (2018).
48. White, J. K., Schmehl, R. H. & Turro, C. An overview of photosubstitution reactions of Ru(II) imine complexes and their application in photobiology and photodynamic therapy. *Inorganica Chimica Acta* **454**, 7–20 (2017).
49. Lee, U. N., Day, J. H., Haack, A. J., Bretherton, R. C., Lu, W., DeForest, C. A., Theberge, A. B. & Berthier, E. Layer-by-layer fabrication of 3D hydrogel structures using open microfluidics. *Lab Chip* **20**, 525–536 (2020).
50. DeForest, C. A., Polizzotti, B. D. & Anseth, K. S. Sequential click reactions for synthesizing and patterning three-dimensional cell microenvironments. *Nat. Mater.* **8**, 659–664 (2009).
51. Rapp, T. L., Phillips, S. R. & Dmochowski, I. J. Kinetics and Photochemistry of Ruthenium Bisbipyridine Diacetonitrile Complexes: An Interdisciplinary Inorganic and Physical Chemistry Laboratory Exercise. *J. Chem. Educ.* **93**, (2016).